Environmental Science & Technology

Article

Cite This: Environ. Sci. Technol. 2019, 53, 3538−3546

pubs.acs.org/est

Nanostructure of Gasification Charcoal (Biochar)

Jacob W. Martin,[†,†] Leonard Nyadong,[¶] Caterina Ducati,[§] Merilyn Manley-Harris,[‖] Alan G. Marshall,[⊥] and Markus Kraft*[,†,‡,#]

[†]Department of Chemical Engineering and Biotechnology, University of Cambridge, Philippa Fawcett Drive, West Site, CB3 0AS Cambridge, U.K.

[‡]Cambridge Centre for Advanced Research and Education in Singapore (CARES), CREATE Tower, 1 Create Way, Singapore 138602

[¶]Phillips 66 Research Center, Highway 60 & 123, Bartlesville, Oklahoma 74003-6607, United States

[§]Department of Materials Science and Metallurgy, University of Cambridge, Philippa Fawcett Drive, West Site, CB3 0FS Cambridge, U.K.

[‖]School of Science, University of Waikato, Hillcrest, Hamilton 3216, New Zealand

[⊥]National High Magnetic Field Laboratory, Florida State University, 1800 E. Paul Dirac Drive, Tallahassee, Florida 32310-4005, United States

[#]School of Chemical and Biomedical Engineering, Nanyang Technological University, 62 Nanyang Drive, Singapore 637459

ABSTRACT: In this work, we investigate the molecular composition and nanostructure of gasification charcoal (biochar) by comparing it with heat-treated fullerene arc-soot. Using ultrahigh resolution Fourier transform ion-cyclotron resonance and laser desorption ionization time-of-flight mass spectrometry, Raman spectroscopy, and high resolution transmission electron microscopy we analyzed charcoal of low tar content obtained from gasification. Mass spectrometry revealed no magic number fullerenes such as C_{60} or C_{70} in the charcoal. The positive molecular ion m/z 701, previously considered a graphitic part of the nanostructure, was found to be a breakdown product of pyrolysis and not part of the nanostructure. A higher mass distribution of ions similar to that found in thermally treated fullerene soot indicates that they share a nanostructure. Recent insights into the formation of all carbon fullerenes reveal that conditions in charcoal formation are not optimal for the formation of fullerenes, but instead, curved carbon structures coalesce into *fulleroid-like* structures. Microscopy and spectroscopy support such a *stacked, fulleroid-like* nanostructure, which was explored using reactive molecular dynamics simulations.

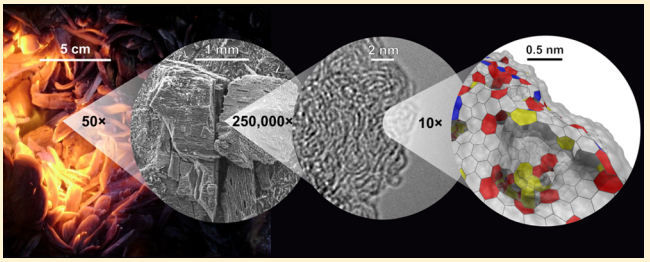

INTRODUCTION

Charcoal is formed from the thermal transformation of a carbon-rich substance, often woody biomass, into a solid carbon product. It has been produced in fires and kilns for millennia and used for creating art, smelting ores to produce metals, and as a smokeless fuel.[1] Recently, advanced applications have been developed for charcoal such as electrode materials for lithium-ion batteries,[2] activated carbons,[3] and supercapacitors.[4] Environmental concerns have also prompted research into charcoal as a carbon capture technology. Storing atmospheric carbon is now possible considering that biomass, as it grows, photosynthetically captures carbon dioxide. Subsequent thermal treatment traps some of that carbon in stable charcoal that will not break down. As this charcoal is also known to enhance crop yields (allowing costs to be offset), many researchers are suggesting the addition of charcoal in order to improve soils while storing carbon.[5,6] Charcoal produced for application to the soil is often called biochar.

One means of offsetting biochar's cost is the production of energy through a process called gasification.[7] The gasification process injects a restricted supply of oxygen into a sealed vessel that oxidizes some of the carbon in the charcoal to produce high temperatures (1000 °C). The surface of the hot carbon is then able to perform the gasification reactions, reducing carbon dioxide and water to carbon monoxide and hydrogen. The hot carbon is also able to crack unburnt hydrocarbons (tar)[8,9] leading to a clean syngas fuel that can power a turbine or internal combustion engine. The high temperatures reached inside a gasifier produce a high quality charcoal with low tar content (low hydrogen content), which is necessary for the long-term stability of the material.[5,10] The nanostructural understanding of gasification charcoal is therefore important

Received: December 6, 2018
Revised: January 18, 2019
Accepted: March 13, 2019
Published: March 13, 2019

DOI: 10.1021/acs.est.8b06861
Environ. Sci. Technol. 2019, 53, 3538−3546

for determining the reactivity of the char to produce syngas and also for considering the long-term stability of such a material for carbon capture and storage. An understanding of the material properties could also stimulate interest in new applications for carbon nanostructured materials produced from natural biomass precursors.

With a concentration on woody biomass and consideration of how it thermally transforms into charcoal in the absence of air (pyrolysis), a dynamic molecular structure has previously been proposed.[11] In this scheme, initially, the crystalline and noncrystalline saccharide precursors dehydrate, decarboxylate, and depolymerize, forming pyrogenic amorphous carbon.[12] An analysis of hydrothermally treated saccharide suggests a pyrogenic structure containing six-membered aromatic rings and species such as hydroxymethylfurfural.[13,14] Ring condensation from 400 to 700 °C leads to the formation of stacked aromatic domains.[15] These small layered turbostratic (graphitic without ideal ABA stacking) disordered regions are completely developed by 700 °C and have been recently imaged in charcoal.[16] At this temperature, the material is nearly entirely composed of carbon (95 wt %). Thermal treatment to 1000 °C further decreases the amount of oxygen to 1−3%, removes any remaining hydrogen (<1 wt %), and increases the graphitic turbostratic domains. The gasification process also includes oxidation and activation of the charcoal during reduction, which reduces density and integrates porosity.[17]

Significant experimental evidence has emerged suggesting a *fullerene-like* nanostructure for charcoal[18] (where a fullerene is a molecule with carbon atoms arranged in a closed network of pentagonal and hexagonal rings[19]). Pentagonal and heptagonal rings have been resolved by use of high resolution transmission electron microscopy (HRTEM) in microporous carbons,[17,20] as well as closed cages and curved fragments in carbon heated to higher temperatures (>1500 °C) such as glassy carbon.[21] A recent review of the nanostructure of nongraphitising carbon, focusing on charcoal in particular, has also highlighted the role of oxygen in inhibiting planarization of the structure,[22] and experimental results have suggested that the mechanism for pentagon integration is the loss of oxygenated fragments along the zigzag edge of aromatic species.[23]

Laser desorption time-of-flight mass spectrometry (LDI-TOF MS) is one of many techniques that have been used to study the structures of these nongraphitising carbons. In a study of graphite, diamond, glassy carbon, carbon nanotubes, and *diamond-like* thin layers, Sedo et al. observed only in glassy carbon, some high intensity, positive ions in the range m/z 400−800, the highest being m/z 701.[24] The ions were discarded as an artifact by the authors but were later observed by Bourke and co-workers in biomass and sugar-derived charcoals prepared with flash pyrolysis at 950 °C.[25] Sedo et al. also found that by increasing the laser power, a distribution of more massive ions was produced. However, the absence of the m/z 720 ion (C_{60} fullerene) in charcoal and also of large even-numbered carbon cages in glassy carbon called into question a *fullerene-like* nanostructure.

In this article, we aim to understand how the mass spectrometry of charcoal, indicating no fullerenes, can be understood in light of the microscopy and spectroscopy, suggesting curved fullerene-like fragments, by comparing a gasification charcoal with thermally treated fullerene-soot, which we have previously studied.[26]

MATERIALS AND METHODS

Production of Charcoal. Untreated *Pinus radiata* wood, sourced from Carter Holt Harvey Wood Products, New Zealand (NZ), was cut into (30 × 30 × 10 mm) blocks which were carbonized with a downdraft gasifier that was custom built based on the microlab class gasifier from Fluidyne Gasification Ltd., NZ. Figure 1 shows the reaction segment of the gasifier. The wood flowed under gravity and was heated from below to be dehydrated and then thermally pyrolyzed into charcoal. Nozzles were then used to inject air, and the charcoal was oxidized. Once the oxygen was consumed, reduction of CO_2 and H_2O occurred on the surface of the hot carbon. Charcoal then dropped through the grate and was collected in the lower chamber.

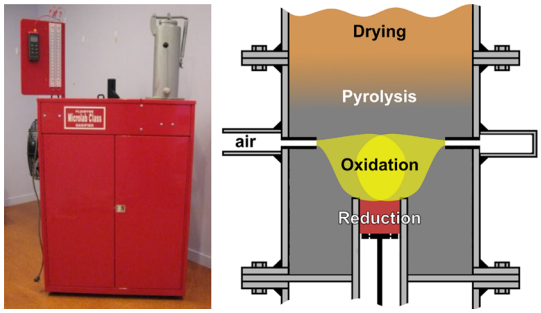

Figure 1. Photograph of the Microlab class gasifier (left). Schematic of the gasifier throat showing the different reaction zones (right). Used with permission from Fluidyne Gasification Ltd., NZ.

Positive pressure was supplied to the air inlet connected to the nozzles, and the gasifier was ignited and run for 20 min. The reactor was then starved of oxygen and cooled for a period of 2 h. Charcoal was taken from the interface between the pyrolysis and oxidation zones, which had yet to undergo significant oxidation and activation but had attained high temperatures. These zones were well separated in the downdraft gasifier that we employed. Charcoal from this region is not significantly oxidized but does not have soot present on its surface, which was determined by a visible change in the charcoal's appearance. Before analysis of the charcoal by LDI-TOF MS, the carbon was stored in evacuated glassware in order to prevent contamination from plasticizers and other environmental species.

Ultimate analysis of the C, H, N, S, and ash percentage weights (wt %) was determined by use of the ASTM D 3176 standard (Table 1). Oxygen wt % was determined through difference and does not include oxygen contained in the ash oxides. The Campbell Micro Analytical Laboratory at the University of Otago conducted the analysis of the oven-dried charcoal.

Table 1. Ultimate Analysis of Gasification Charcoal (wt %)

C	H	O	N	Ash
90.80	<0.1	3.34	<0.1	5.8

The charcoal prepared in this study was found to contain 3.34% oxygen. This is consistent with the flash pyrolysis process which produced charcoals with oxygen contents between 2 and 5% at 950 °C.[25] A low percentage of hydrogen was found in the structure, indicating tar is not present in the charcoal, i.e., a highly cross-linked nanostructure.

DOI: 10.1021/acs.est.8b06861
Environ. Sci. Technol. 2019, 53, 3538−3546

LDI-TOF Mass Spectrometry of Charcoal. A Bruker UltrafleXtreme matrix-assisted laser desorption ionization time-of-flight/time of flight (MALDI-TOF/TOF) mass spectrometer was used for characterizing the positive ions corresponding to the mass distribution of carbon fragments. Ions were produced by use of a nanosecond pulsed 355 nm frequency-tripled Nd:YAG laser (1 kHz repetition rate, 5 ns pulse duration, maximum power of 2.3 μJ, spot size of 100 μm with a maximum laser fluence of 29.3 mJ/cm^2). The Bruker Peptide calibration standard was used to calibrate the instrument.

ESI FT 9.4 T ICR Mass Spectrometry. For analysis, the charcoal sample was ground into a fine powder with a mortar and pestle. A 700 mg portion of the powder was suspended in 30 mL of toluene and sonicated for three hours to extract any soluble sample components. Two mL aliquots were placed in four centrifuge tubes; the aliquots were centrifuged for 30 min, and the supernatant (stock solution) was pulled. For (+) electrospray ionization (ESI) analysis, the stock solution was diluted with methanol to a final composition of 50:50 MeOH/stock with 1% HCOOH modifier and analyzed by ESI Fourier transform ion cyclotron resonance mass spectrometry (FT-ICR MS) at the National High Magnetic Field Laboratory, Florida State University.

Raman Spectroscopy. The Raman spectrometer (Horiba Jobin Yvon LabRAM HR) was equipped with an Olympus BX41 microscope (×10 objective). The instrument was calibrated based on the 520.5 cm^{-1} line of silicon. Raman spectra were excited by a Nd:YAG laser (532.8 nm, 16 mW) at a nominal resolution of 4−6 cm^{-1} in the 1000−1800 cm^{-1} range. The acquisition was repeated four times with an exposure time of 8 s to improve the signal-to-noise ratio. A linear baseline was applied to the graph which was optimized as the peaks were fitted ($ax + b$; $a = 0.405 \pm 0.003$, $b = 985 \pm 5$).

The fitting procedure was based on the work by Smith et al., who applied electronic structure calculations to a variety of aromatic molecules with defects and nonhexagonal rings.[27] Each species was found to have Raman excitations at many different frequencies. Due to the variety of carbon structures and defective carbon in charcoal it would be appropriate to fit regions of the spectrum with Gaussian functions rather than fitting a single Lorentzian. This was justified by supposing that very disordered materials will have a random distribution of Lorentzian functions about each major resonance which would have a Gaussian shape. In chars prepared at lower temperatures, the ring vibrations indeed display a more Gaussian profile.[27] Structures with more homogeneous aromatic molecules, such as in soot, show more of a Lorentzian profile, and the fitting of a single Lorentzian to each is more justified. The goal then of fitting regions with Gaussian functions is to quantify the amount of certain types of defects determined from electronic structure calculations. It should be noted, however, that the conclusions made are also found if Lorentzian functions are used instead of Gaussian functions for the D and G bands as there is still substantial intensity between the D and G band which is usually fitted by use of a smaller Gaussian function.

High Resolution Transmission Electron Microscopy. Images were captured by a FEI^{TM} Tecnai F20 which operated at an accelerating voltage of 200 kV. This instrument is equipped with a SuperTwin objective lens with a C_S of 1.2 mm. Images were captured with a Gatan imaging filter (GIF) 200, fitted with a 1k × 1k CCD digital camera. Phase contrast high resolution TEM images with 0.2 nm resolution were obtained from graphitic regions that were oriented so that their basal planes were at Bragg angles with the electron beam. Charcoal was gently ground in a mortar and pestle. This did not alter the nanostructure of the carbon significantly, as noted by Harris et al.[28] The carbon was then suspended in a solution of isopropyl alcohol and was placed on a C-Flat^{TM} Holey carbon support with holes that were one micron in diameter, and only regions extending into the vacuum were imaged.

Model Construction. We made use of a molecular geometry from the work of de Tomas et al.[30] (made accessible on the Web site carbonpotentials.org). This geometry was produced from a quenched molecular dynamics simulation by use of the REBO-II reactive potential in a periodic 7.58 nm wide cube[29] with periodic boundary conditions. In order to describe the surface, the geometry was sliced along the diagonal and an NVT molecular dynamics simulation was performed in the LAMMPS software package[31] with the same reactive force field. The Nose-Hoover chain thermostat was used to maintain a system temperature of 3000 K. A time step of 0.5 fs was used with a total simulation time of 3.6 ns. In order to close the defective graphene that would normally be attached to the periodic image, the simulation box was extended past the carbon structure to allow the surfaces to anneal. Figure 2 shows the molecular geometry. The nonhexagonal rings were determined by use of the algorithm developed by Franzblau.[32] Polypy, a python program by Jaap Kroes (https://github.com/jaapkroe/polypy), was used to

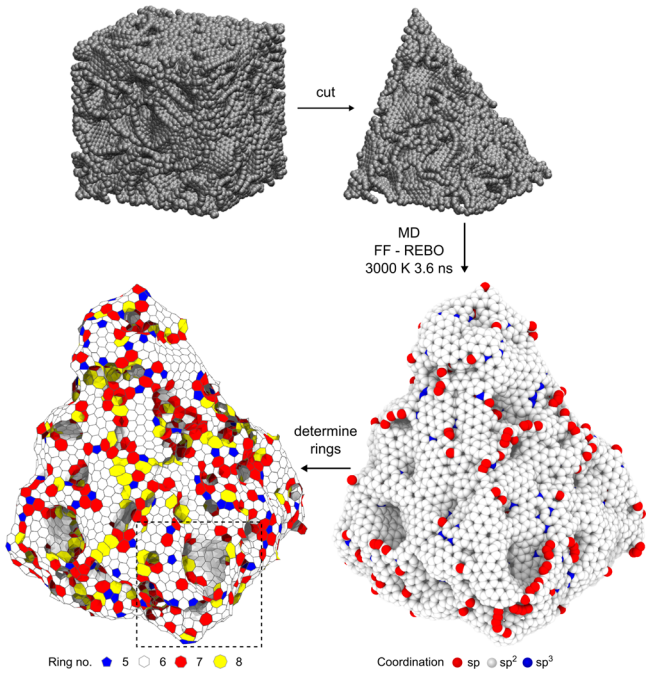

Figure 2. Protocol for preparing the molecular geometry. A three-dimensional periodic model prepared using the REBO force field[29] was used from de Tomas et al.[30] The corner was cut and the surface was annealed using the same force field for 3.6 ns at 3000 K to anneal the surface. The structure is shown colored by the coordination number (2, red; 3, white; 4, blue). The different rings were then determined and are colored according to ring number (5, blue; 6, white; 7, red; 8, yellow). An expanded image of dashed box around the region is shown in Figure 7.

DOI: 10.1021/acs.est.8b06861
Environ. Sci. Technol. 2019, 53, 3538−3546

generate the colored polygons, and the software visual molecular dynamics VMD was used to render the geometry.[33]

HRTEM images of this carbon model were generated using the multislice method. The software detailed in the book *Advanced Computing in Electron Microscopy* by Kirkland[34] was used to simulate the propagation and scattering of electrons through the molecular structure. Parameters used for the simulation were an accelerating voltage of 200 kV, objective aperture of 20 mrad, and a defocus of 20 nm.

RESULTS AND DISCUSSION

High Resolution Mass Spectrometry. Charcoal was taken from the interface of the pyrolysis and oxidation zones where temperatures of 1000 °C were attained (as measured via a K-type thermocouple) and soot was not present on the char in this region, which allowed the solid state charcoal to be resolved without interference from soot produced in the gas phase. Figure 3 shows the LDI-TOF mass spectrum of charcoal

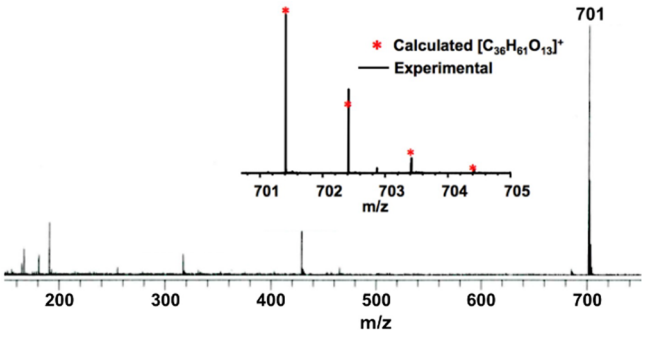

Figure 3. LDI-MS low mass positive ions from m/z 150−850 for gasification charcoal, showing the prominent m/z 701. Inset right: a mass-scale expanded segment with mass-to-charge (m/z) in the range 700−705 following positive-ion ESI 9.4 T FT-ICR mass spectrometry analysis of a toluene charcoal extract. Represented by an asterisk is the calculated isotopic distribution for the species with elemental formula $C_{36}H_{61}O_{13}$ corresponding to the peak assignment.

with a low laser fluence (10.3 mJ/cm^2), providing ions with the prominent peak at m/z 701 and low abundances of other ions compared to flash pyrolysis, indicating low amounts of extractable tars and no magic number fullerenes C_{60} or C_{70}.[25] Elemental analysis also revealed low amounts of hydrogen, further indicating low tar, highly cross-linked, and well developed nanostructure.

To resolve the elemental structure of the m/z 701 ion and determine if the ion is a constituent of the nanoscale structure, high resolution mass spectrometry was used. Toluene was used to extract the species. The extract was then injected into the electrospray ionization ion source and analyzed by a 9.4 T Fourier transform ion cyclotron resonance mass spectrometer (ESI 9.4 T FT-ICR MS). The inset in Figure 3 shows the experimental mass spectrum with the various isotopic peaks for the ion, with a measured accurate mass of 701.4092 Da. While wood contains a variety of elements, the presence of the m/z 701 ion in feedstocks containing only C, H, and O, studied previously by the authors and others,[24,25] led us to propose $[C_{36}H_{60}O_{13}+H]^+$ as the candidate ion of which the difference between measured and calculated mass is 1.1 ppm. The candidate ion's elemental formula contains a significant amount of hydrogen and oxygen, indicating that the ion is not aromatic but an early breakdown product of pyrolysis. The elemental composition determined from the ultimate analysis indicated significantly less hydrogen and oxygen in the material that would suggest a highly aromatic nanostructure (Table 1). Further analysis of the LDI-TOF mass spectrum of charcoal after passing through the entire gasification reactor showed the loss of the m/z 701 ion, indicating that it was broken down during the gasification process. Charcoals containing the m/z 701 ion were also sensitive to oxygen with exposure to air, leading to the loss of the ion after two to three months. These results support the conclusion that the m/z 701 ion is an unstable trace product of pyrolysis and is not part of the nanostructure. The FT-ICR MS analysis also confirmed that there were no detectable amounts of magic number fullerenes such as C_{60} or C_{70} in this gasification charcoal.

Considering the LDI-TOF MS experiment again, we found that by increasing the laser fluence (12.8 mJ/cm^2), a distribution of higher m/z ions could be observed that is similar to that found for thermally treated fullerene soot.[26] Figure 4a shows the skewed distribution of peaks. Figure 4b shows an enlarged region of the mass spectrum showing that the distribution is made up of a collections of peaks that are separated by m/z 24 (C_2). The isotopic peaks are indicative of predominately carbon species with one, two, and three oxygen atoms that are integrated, and the lack of intensity between these collection of peaks indicates that no all-carbon fullerene cage ions are present and these species are not dimers, trimers, etc. of PAHs.

We have previously found a similar distribution of oxygenated fragments separated by m/z 24 in thermally treated fullerene arc-carbon where oxygen present in the structure, from exposure to air, became chemically integrated into a cross-linked curved nanostructure upon heating.[26] Figure 4b shows an enlarged region of the mass spectrum showing triplicate peaks of oxygenated ions. For comparison, the same region is shown in Figure 4c for thermally treated fullerene soot we previously collected[26] which shows a similar triplicate separated by m/z 24.

Care must be taken, however, when analyzing such a mass distribution in gasification charcoal due to the possibility of modifying the structure as a result of laser ablation.[35] We ensured that no fragmentation could be observed under m/z 200 for charcoal, which we have previously found to modify the distribution of higher ions found in fullerene soot.[26] By ablating graphite at the maximum laser fluence, we produced these small fragments and did not observe fullerene ions, indicating that the laser desorption process and vacuum chamber were not conducive to fullerene formation.[26] Another important consideration is that laser ablation could produce hot fragments that could close curved fragments in the gas phase.[36] With these caveats, the similarities between the mass spectra of charcoal and thermally treated fullerene soot indicate a shared, curved nanostructure.

Raman Spectroscopy. Raman scattering was also used to analyze the structure. The Horiba LabRam Raman microscope, equipped with a 532 nm laser, provided excitation of the sample, and spectra were collected near the ring breathing modes (1000−1800 cm^{-1}) of the graphitic carbon. Recent electronic structure calculations of the vibrational frequencies for various defective polycyclic aromatic hydrocarbons have provided insights into fitting this highly structured region of the Raman spectrum for charcoal.[27,37,38] In particular, the region from 1400 to 1460 cm^{-1} has been suggested to arise from the breathing mode of 5-membered rings.[27,38]

DOI: 10.1021/acs.est.8b06861
Environ. Sci. Technol. 2019, 53, 3538−3546

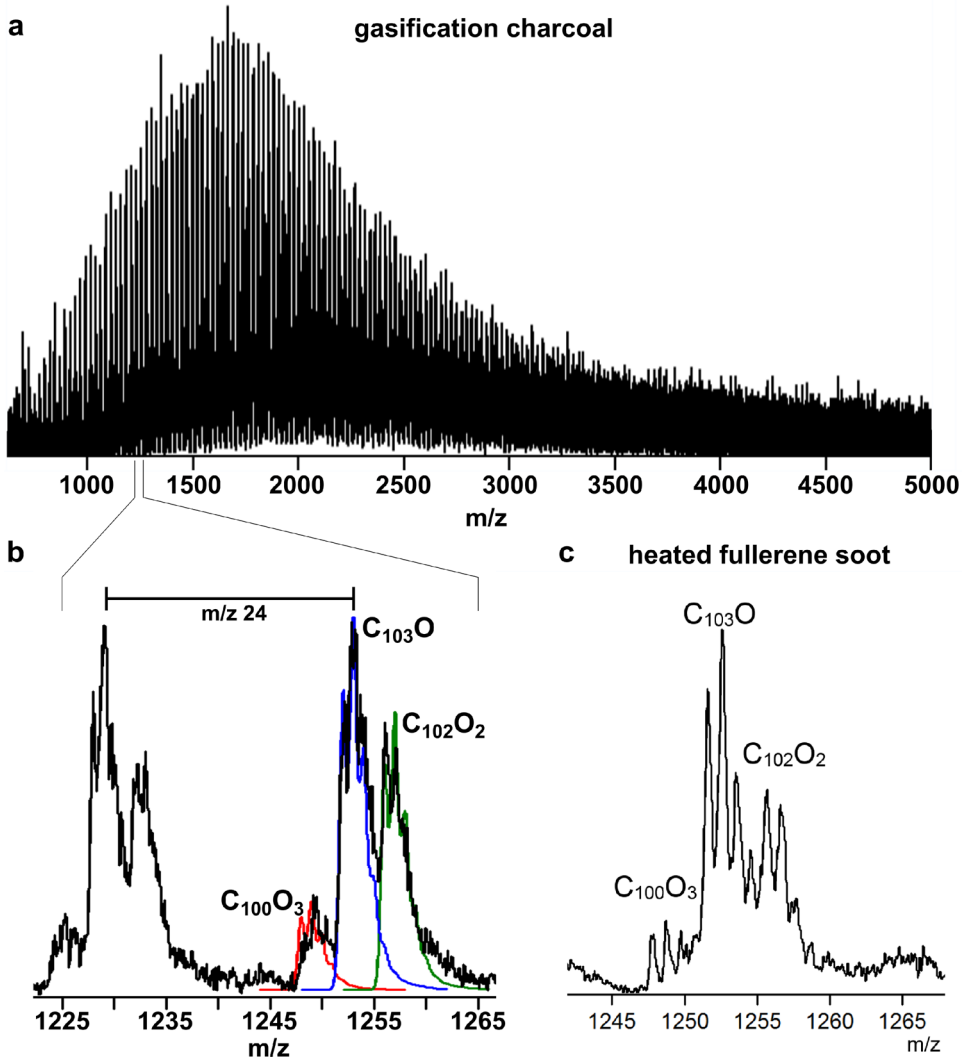

Figure 4. (a) LDI-TOF-MS mass spectrum of charcoal at high laser fluence (12.8 mJ/cm^2). A distribution of peaks is observed separated by m/z 24. (b) Region between m/z 1245−1265 with three species isotope-simulated responses overlaid (colored). (c) Similar m/z region of the mass spectrum for heated fullerene soot showing similar oxygenated fragments from Martin et al.[26]

Figure 5 shows the Raman spectrum after baseline correction with the peaks from least-squared fitting (values and errors in the fitted values can be seen in Table 2). We did not observe as much structure in the gasification charcoal Raman spectrum due to the higher temperature treatment compared with the Raman spectrum collected for cellulose char heated from 400 to 700 °C by Smith et al.[27] In particular, the S_L and D_S bands could not be observed. We also found that the S band appeared to contain a strongly Lorentzian tail on the lower wavenumber shoulder, leading us to fit the S peak with a Lorentzian. We were unable to fit two A peaks as has previously been fitted for Raman spectra of wood charcoal prepared via pyrolysis by Smith et al.[27] We fit the A_1 peak, which corresponds to the breathing mode of the 5-membered carbon structures. Fitting a single Gaussian peak between the D and G band provided a peak position of 1457 cm^{-1} which was closer to the A_1 peak (1400−1460 cm^{-1}) than the A_2 peak (1480−1550 cm^{-1}). This led us to assign this peak to the A_1 breathing mode of 5-membered rings. We were unable to fit a second peak (A_2) in this region, previously attributed to sp^2 defects,[27] which we consider as another indicator of the high cross-linking in the sample. We also did not observe the same

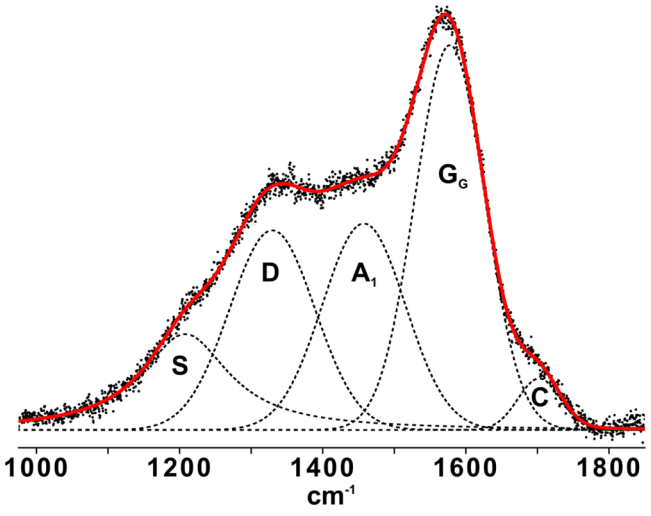

Figure 5. Raman spectrum (532 nm excitation) for gasification charcoal (black points) with the peaks used to fit the spectrum shown (dotted line). The fit is shown (red line). For peak assignments see Table 2.

DOI: 10.1021/acs.est.8b06861
Environ. Sci. Technol. 2019, 53, 3538−3546

Table 2. Peak Assignments and Fitted Parameters[a]

Position	Width	Peak	Shape	Assignment
1209 ± 3	138 ± 7	S	Lorentzian	breathing mode for 7-membered rings or small PAHs or breathing modes adjacent to heteroatom defects.
1329 ± 4	138 ± 11	D	Gaussian	combined breathing modes for PAHs
1457 ± 2	115 ± 1	A_1	Gaussian	breathing mode for 5-membered rings
1577 ± 1	141 ± 3	G_G	Gaussian	asymmetric vibrations for small PAHs
1702 ± 1	67 ± 2	C	Gaussian	carbonyl stretching mode

[a]Values in cm^{-1}.

shoulder on the lower wavenumber side of the G peak as seen in low temperature charcoal,[27] further indicating the lack of the A_2 peak. The high temperature treatment appears to have significantly reduced or removed the peaks associated with disordered carbon such as the A_2 and S_L.

A strong C peak was also observed at 1702 cm^{-1} indicative of carbonyl species. Due to this peak, the Lorentzian tail on the higher wavenumber shoulder could not be fitted with a second G_L Lorentzian that describes the E_{2g} mode for larger PAHs. In comparison with the low temperature charcoal, this strong C band indicates a larger amount of carbonyl oxygen species. This would align with our observation of the thermal treatment of fullerene soot with oxygen that converted to carbonyl species.[26]

High Resolution Transmission Electron Microscopy. Electron microscopy also indicated such a curved structure. We found that the lack of un-cross-linked extractable fraction (liquid tar) in the gasification charcoal improved the stability of the structure under the electron beam. Figure 6 shows transmission electron micrographs along the edges of different regions of the charcoal protruding into the vacuum where observation of the geometry was least obscured. Figure 6a shows a low magnification image of the edge of a charcoal particle. Curved regions can be seen around the edge. Figure 6b,c shows higher magnification images. An *onion-like* structure can be observed in panel b. At the highest magnification, curved nanostructures with radii of curvature up to 1 nm are observed. Alongside the curved structures, regions of layered graphitic planes can also be observed.

Curved structures have been previously observed in HRTEM of charcoal;[2,39] multiwalled curved *onion-like* structures were also seen in HRTEM[40] and scanning probe microscopy.[41] This curved nanostructure was similar to that found for sucrose char heated to 1000 °C in an inert environment with a curved isotropic arrangement of fringes and dissimilar to that found for anthracene carbonized under similar conditions that produced an anisotropic arrangement of fringes with a low degree of curvature.[18]

We first discuss the reason for the absence of the magic number fullerenes, which previously led one to doubt a fullerene-like nanostructure for charcoal.[25] Recent advances in the understanding of magic number fullerene formation might help to explain why such species are unlikely to be found in charcoal.[26,42−45] Synthesis conditions required for magic number fullerenes are high-energy, nonequilibrium, dissipative environments such as those in carbon arcs or low pressure oxygen-benzene combustion.[46] These environments allow curved aromatic structures to form that eventually close into disordered fullerenes.[42] The high-energies allow cages to eject and gain C_2.[43−45,47] During this shrinking (C_2 ejection)[42] and closed network growth (C_2 gain),[45] the magic number fullerenes can be produced in high abundance due to the larger energy barriers for C_2 loss or gain from these symmetric cages compared with their neighbors, i.e., residing in *local* energy minima as shown by Curl et al.[44]

In contrast to the gas-phase synthesis, we previously found that when arc-produced magic number fullerenes in the solid state were heated, magic number fullerenes were consumed and they coalesced into giant fullerenes.[26] The ability of curved carbon nanostructures to fuse and coalesce is well-known, for example, the coalescence of fullerenes inside nanotubes leads to double walled nanotubes,[48] and the fusing of single walled nanotubes into multiwalled nanotubes has been shown.[49] This reactivity was studied via electronic structure methods and found to be due to the pyramidalization of the carbon atoms which reduces the aromaticity around the defect and allows sp^3 bonds to be formed fusing the curved regions.[4,26,50] Importantly, the temperatures in most charcoal production do not reach those necessary to evaporate C_2, which is needed for evaporation of C_2 to form small magic number fullerenes. Therefore, if curved *fullerene-like* fragments are present in gasification charcoal, the synthesis conditions would not be conducive to magic number fullerene formation.

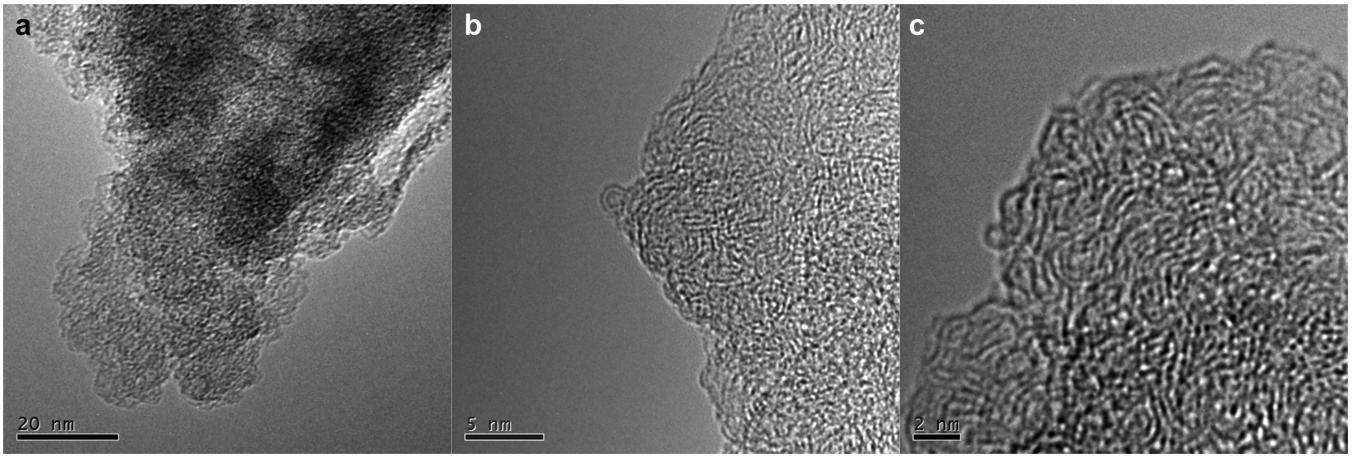

Figure 6. HRTEM images of gasification charcoal taken at 200 kV accelerating voltage.

DOI: 10.1021/acs.est.8b06861
Environ. Sci. Technol. 2019, 53, 3538−3546

Upon consideration of the LDI TOF MS higher mass distribution of ions (Figure 4), we found for charcoal with an increase in laser intensity, we considered potential interpretations of what this distribution indicated about the nanostructure. One option could be that the distribution is due to dimers, trimers, tetramers etc.; of predominantly planar stacked aromatic layers with oxygen functionalization. We think this is unlikely for a few reasons. First, the monomodal distribution is indicative of a continuous solid. Cross-linking of small PAHs is known to yield a multimodal distribution of peaks with a periodicity relating to the average molecular mass of the subunits.[51] Physical clustering in the case of aromatic molecules in soot formation is also known to lead to a multimodal distribution.[52] Second, the separation of the peaks by m/z 24 and the amount of oxygen per carbon peak is indicative of a similar curved nanostructure between heat treated fullerene soot and charcoal, which are both able to form fragments that close into oxygenated cages upon ablation. Third, our previous study showed that ablation of the microcrystalline graphite containing planar carbon did not lead to formation of a distribution of peaks separated by m/z 24 as well as a lack of C_{60} and C_{70}, indicating that the laser power and vacuum inside the mass spectrometer are unable to produce fragmentation products and fullerenes when ablated.[26] However, from the HRTEM, we do see evidence of the stacking of aromatic layers interacting via van der Waals forces. One suggestion for why this stacking is not reflected in the mass spectrum could be due to an effect that Marsh commented on when discussing activated carbons[53]—many experimental techniques that probe carbon's nanostructure, such as HRTEM and X-ray diffraction, are most sensitive to regions where aromatic sheets are stacked; however, these sheets should extend past the stacked regions. This would lead to an underestimation of the aromatic network from considering only the stacked regions and not the single layers. The mass spectrum and HRTEM are consistent with a continuous curved nanostructure with regions of layering.

Figure 7 shows a molecular nanostructure which aims to consider the possible structures present in gasification charcoal generated from a modified quenched molecular dynamics study.[30] We have chosen not to consider oxygen in the model as it is only a minor component and therefore does not correspond to the long-range graphitic nanostructure. The low amount of hydrogen in the elemental composition led us to consider a model that contained only carbon. Figure 7a shows the surface of the nanostructure with the nonhexagonal rings that form due to the closure of the surface that is shown as colored. Both pentagonal rings that provide bowl-shaped surfaces and rings with greater than six rings that provide saddle-shaped geometries were observed, which allow for a large proportion of nonreactive sp^2 carbon atoms to be assembled at the surface. The effectiveness of the nanostructure closure is seen in Figure 2 where atoms are colored by coordination, revealing low numbers of reactive edges. We are currently exploring how this could confer oxidation resistance to biochar.

Figure 7b,c shows the simulated HRTEM images of the model produced, using the multislice method, for two different orientations. Fringes with similar degrees of curvature (radii of curvature of ∼1 nm) were found. Some stacking was also observed for Figure 7c. Significant improvements could be made to such a model to ensure quantitative agreement between the model and the experimental HRTEM; however,

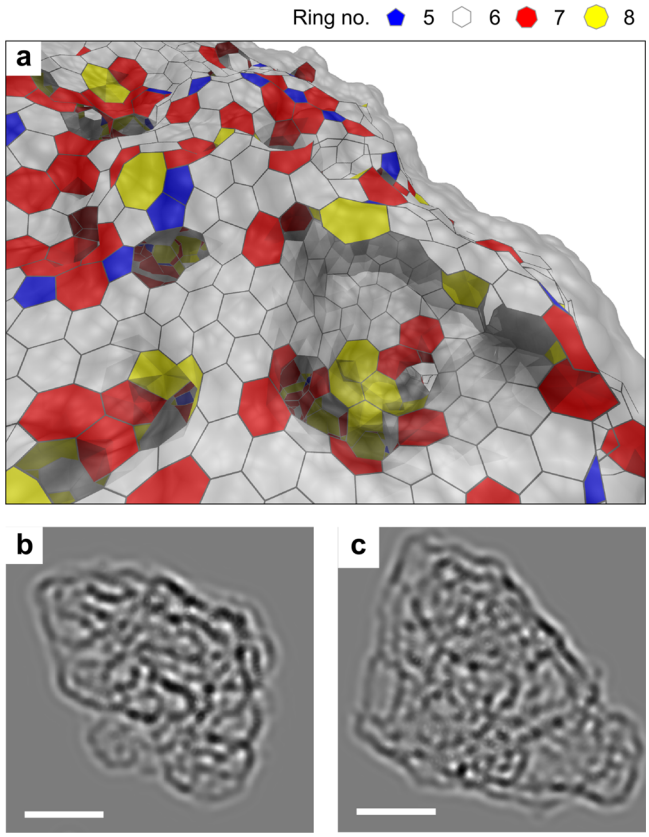

Figure 7. (a) Proposed *stacked, fulleroid-like* molecular nanostructure model for charcoal with rings colored blue, white, red and yellow for 5-, 6-, 7- and 8-membered rings, respectively (the dashed box in Figure 2 shows the location of this expanded section). (b, c) Simulated HRTEM images of the model structure with 2 nm scale bars shown.

we have shown here a preliminary model which is able to demonstrate the main features of the HRTEM of significantly curved fringes, with some stacked fringes and with low amounts of unsaturated sp and sp^3 hybridized carbon.

These nonhexagonal rings have been directly imaged in wood charcoal using aberration-corrected HRTEM as mentioned in the Introduction.[20] We consider these topological defects to be present within a three-dimensional graphene network. When we considered what to call such a structure, we decided not to refer to the structure as *fullerene-like* (fullerenes are defined as closed triply connected carbon networks containing pentagonal and hexagonal rings[19]) and instead used the term *fulleroid-like* (fulleroid refers to a closed carbon network containing rings with any number of carbon atoms[19,54]). A *stacked, fulleroid-like* nanostructure could form an extended porous, curved, *foam-like* nanostructure with enclosed fulleroids and regions of layering.

We have previously shown that large electric fields are present around regions of positive Gaussian curvature in pericondensed aromatics.[55] These regions would be present in such a *stacked, fulleroid-like* structure. Understanding how the flexoelectric effect impacts adsorption properties of charcoal and activated carbon could provide considerable insight into their ability to adsorb ions and polar species. Further work is also needed to determine how oxygen is integrated into charcoal's nanostructure with its presence in all higher ions

DOI: 10.1021/acs.est.8b06861
Environ. Sci. Technol. 2019, 53, 3538−3546

desorbed from charcoal indicating that it is a part of the *stacked, fulleroid-like* nanostructure.

AUTHOR INFORMATION

Corresponding Author

*E-mail: mk306@cam.ac.uk. Phone: +44 (0)1223 762784.

ORCID

Jacob W. Martin: 0000-0002-7514-4549
Leonard Nyadong: 0000-0003-4701-1519
Alan G. Marshall: 0000-0001-9375-2532
Markus Kraft: 0000-0002-4293-8924

Notes

The authors declare no competing financial interest.

ACKNOWLEDGMENTS

This project is supported by the National Research Foundation (NRF), Prime Minister's Office, Singapore under its Campus for Research Excellence and Technological Enterprise (CREATE) programme, and the U.S.A. National Science Foundation Division of Materials Research through DMR-11-57490h. The authors thank Robert Curl (Rice University) and Brian Nicholson (University of Waikato) for their helpful discussions, Angus Grey (University of Auckland) for his expertise with the LDI-TOF MS, Doug Williams (Fluidyne Gasification Ltd) and Peter Wilkinson (Wilkinson Transport Engineers) for the gasifier design and construction, and Nigel Marks, Irene Suarez-Martinez, and Carla de Tomás (Curtin University) for providing the annealed molecular dynamics models, which were modified as shown in this document.

REFERENCES

(1) Antal, M. J.; Grønli, M. The art, science, and technology of charcoal Production. *Ind. Eng. Chem. Res.* **2003**, *42*, 1619−1640.

(2) Liu, T.; Luo, R.; Qiao, W.; Yoon, S.-H.; Mochida, I. Microstructure of carbon derived from mangrove charcoal and its application in Li-ion batteries. *Electrochim. Acta* **2010**, *55*, 1696−1700.

(3) Benedetti, V.; Patuzzi, F.; Baratieri, M. Gasification Char as a Potential Substitute of Activated Carbon in Adsorption Applications. *Energy Procedia* **2017**, *105*, 712−717.

(4) Xu, L.; Yao, Q.; Zhang, Y.; Fu, Y. Integrated production of aromatic amines and N-Doped carbon from lignin via ex situ catalytic fast pyrolysis in the presence of ammonia over zeolites. *ACS Sustainable Chem. Eng.* **2017**, *5*, 2960−2969.

(5) Lehmann, J.; Gaunt, J.; Rondon, M. Bio-char sequestration in terrestrial ecosystems a review. *Mitigation and Adaptation Strategies for Global Change* **2006**, *11*, 403−427.

(6) Paustian, K.; Lehmann, J.; Ogle, S.; Reay, D.; Robertson, G. P.; Smith, P. Climate-smart soils. *Nature* **2016**, *532*, 49−57.

(7) Creutzig, F.; et al. Bioenergy and climate change mitigation: An assessment. *GCB Bioenergy* **2015**, *7*, 916−944.

(8) Asadullah, M.; Zhang, S.; Min, Z.; Yimsiri, P.; Li, C. Z. Effects of biomass char structure on its gasification reactivity. *Bioresour. Technol.* **2010**, *101*, 7935−7943.

(9) Min, Z.; Yimsiri, P.; Asadullah, M.; Zhang, S.; Li, C.-Z. Catalytic reforming of tar during gasification. Part II. Char as a catalyst or as a catalyst support for tar reforming. *Fuel* **2011**, *90*, 2545−2552.

(10) Spokas, K. A. Review of the stability of biochar in soils: predictability of O:C molar ratios. *Carbon Manage.* **2010**, *1*, 289−303.

(11) Keiluweit, M.; Nico, P. S.; Johnson, M. G.; Kleber, M. Dynamic molecular structure of plant biomass-derived black carbon (biochar). *Environ. Sci. Technol.* **2010**, *44*, 1247−1253.

(12) Lin, Y.-c.; Cho, J.; Tompsett, G. a.; Westmoreland, P. R.; Huber, G. W. Kinetics and mechanism of cellulose pyrolysis. *J. Phys. Chem. C* **2009**, *113*, 20097.

(13) Baccile, N.; Falco, C.; Titirici, M. M. Characterization of biomass and its derived char using 13C-solid state nuclear magnetic resonance. *Green Chem.* **2014**, *16*, 4839−4869.

(14) Titirici, M.-M.; White, R. J.; Falco, C.; Sevilla, M. Black perspectives for a green future: hydrothermal carbons for environment protection and energy storage. *Energy Environ. Sci.* **2012**, *5*, 6796.

(15) Inagaki, M.; Kang, F. *Materials science and engineering of carbon: fundamentals*; Butterworth-Heinemann: 2014.

(16) Xiao, X.; Chen, B. A direct observation of the fine aromatic clusters and molecular structures of biochars. *Environ. Sci. Technol.* **2017**, *51*, 5473−5482.

(17) Harris, P. J. F.; Liu, Z.; Suenaga, K. Imaging the atomic structure of activated carbon. *J. Phys.: Condens. Matter* **2008**, *20*, 362201.

(18) Harris, P. J. F. New perspectives on the structure of graphitic carbons. *Crit. Rev. Solid State Mater. Sci.* **2005**, *30*, 235−253.

(19) Schwerdtfeger, P.; Wirz, L. N.; Avery, J. The topology of fullerenes. *Wiley Interdisciplinary Reviews: Computational Molecular Science* **2015**, *5*, 96−145.

(20) Guo, J.; Morris, J. R.; Ihm, Y.; Contescu, C. I.; Gallego, N. C.; Duscher, G.; Pennycook, S. J.; Chisholm, M. F. Topological Defects: Origin of Nanopores and Enhanced Adsorption Performance in Nanoporous Carbon. *Small* **2012**, *8*, 3283−3288.

(21) Harris, P. J. F. Fullerene-related structure of commercial glassy carbons. *Philos. Mag.* **2004**, *84*, 3159−3167.

(22) McDonald-Wharry, J. S.; Manley-Harris, M.; Pickering, K. L. Reviewing, combining, and updating the models for the nanostructure of non-graphitizing carbons produced from oxygen-containing precursors. *Energy Fuels* **2016**, *30*, 7811−7826.

(23) Abrahamson, J. P.; Jain, A.; van Duin, A. C.; Vander Wal, R. L. Carbon structure and the resulting graphitizability upon oxygen evolution. *Carbon* **2018**, *135*, 171−179.

(24) Šedo, O.; Alberti, M.; Janča, J.; Havel, J. Laser desorption-ionization time of flight mass spectrometry of various carbon materials. *Carbon* **2006**, *44*, 840−847.

(25) Bourke, J.; Manley-Harris, M.; Fushimi, C.; Dowaki, K.; Nunoura, T.; Antal, M. J. Do all carbonized charcoals have the same chemical structure? 2. a model of the chemical structure of carbonized charcoal. *Ind. Eng. Chem. Res.* **2007**, *46*, 5954−5967.

(26) Martin, J. W.; McIntosh, G. J.; Arul, R.; Oosterbeek, R. N.; Kraft, M.; Söhnel, T. Giant fullerene formation through thermal treatment of fullerene soot. *Carbon* **2017**, *125*, 132−138.

(27) Smith, M. W.; Dallmeyer, I.; Johnson, T. J.; Brauer, C. S.; McEwen, J.-S.; Espinal, J. F.; Garcia-Perez, M. Structural analysis of char by raman spectroscopy: improving band assignments through first principle computational calculations. *Carbon* **2016**, *100*, 678−692.

(28) Harris, P. J. F. Fullerene-like models for microporous carbon. *J. Mater. Sci.* **2013**, *48*, 565−577.

(29) Brenner, D. W.; Shenderova, O. a.; Harrison, J. a.; Stuart, S. J.; Ni, B.; Sinnott, S. B. A second-generation reactive empirical bond order (REBO) potential energy expression for hydrocarbons. *J. Phys.: Condens. Matter* **2002**, *14*, 783−802.

(30) de Tomas, C.; Suarez-Martinez, I.; Marks, N. A. Graphitization of amorphous carbons: A comparative study of interatomic potentials. *Carbon* **2016**, *109*, 681−693.

(31) Plimpton, S. Fast parallel algorithms for short-range molecular dynamics. *J. Comput. Phys.* **1995**, *117*, 1−19.

(32) Franzblau, D. S. Computation of ring statistics for network models of solids. *Phys. Rev. B: Condens. Matter Mater. Phys.* **1991**, *44*, 4925−4930.

(33) Humphrey, W.; Dalke, A.; Schulten, K. VMD: Visual molecular dynamics. *J. Mol. Graphics* **1996**, *14*, 33−38.

(34) Kirkland, E. J. *Advanced Computing in Electron Microscopy*; Springer US: Boston, MA, 2010.

(35) Dunk, P. W.; Niwa, H.; Shinohara, H.; Marshall, A. G.; Kroto, H. W. Large fullerenes in mass spectra. *Mol. Phys.* **2015**, *113*, 2359−2361.

DOI: 10.1021/acs.est.8b06861
Environ. Sci. Technol. 2019, 53, 3538−3546

(36) Chuvilin, A.; Kaiser, U.; Bichoutskaia, E.; Besley, N. a.; Khlobystov, A. N. Direct transformation of graphene to fullerene. *Nat. Chem.* **2010**, *2*, 450−453.
(37) McDonald-Wharry, J.; Manley-Harris, M.; Pickering, K. Carbonisation of biomass-derived chars and the thermal reduction of a graphene oxide sample studied using Raman spectroscopy. *Carbon* **2013**, *59*, 383−405.
(38) Alvaro Galué, H. Decoding the infrared signatures of pyramidal carbons in graphenic molecular nanostructures of interstellar origin. *Chemical Science* **2014**, *5*, 2667−2676.
(39) Deldicque, D.; Rouzaud, J.-N.; Velde, B. A Raman HRTEM study of the carbonization of wood: A new Raman-based paleothermometer dedicated to archaeometry. *Carbon* **2016**, *102*, 319−329.
(40) Hata, T.; Imamura, Y.; Kobayashi, E.; Yamane, K.; Kikuchi, K. Onion-like graphitic particles observed in wood charcoal. *J. Wood Sci.* **2000**, *46*, 89−92.
(41) Kurosaki, F.; Ishimaru, K.; Hata, T.; Bronsveld, P.; Kobayashi, E.; Imamura, Y. Microstructure of wood charcoal prepared by flash heating. *Carbon* **2003**, *41*, 3057−3062.
(42) Irle, S.; Zheng, G.; Wang, Z.; Morokuma, K. The C_{60} formation puzzle "solved": QM/MD simulations reveal the shrinking hot giant road of the dynamic fullerene self-assembly mechanism. *J. Phys. Chem. B* **2006**, *110*, 14531−14545.
(43) Saha, B.; Irle, S.; Morokuma, K. Hot giant fullerenes eject and capture C_2 molecules: QM/MD simulations with constant density. *J. Phys. Chem. C* **2011**, *115*, 22707−22716.
(44) Curl, R. F.; Lee, M. K.; Scuseria, G. E. C_{60} Buckminsterfullerene High Yields Unraveled. *J. Phys. Chem. A* **2008**, *112*, 11951−11955.
(45) Dunk, P. W.; Kaiser, N. K.; Hendrickson, C. L.; Quinn, J. P.; Ewels, C. P.; Nakanishi, Y.; Sasaki, Y.; Shinohara, H.; Marshall, A. G.; Kroto, H. W. Closed network growth of fullerenes. *Nat. Commun.* **2012**, *3*, 855−859.
(46) Homann, K. H. Fullerenes and soot formation - New pathways to large particles in flames. *Angew. Chem., Int. Ed.* **1998**, *37*, 2434−2451.
(47) Huang, J. Y.; Ding, F.; Jiao, K.; Yakobson, B. I. Real Time Microscopy, Kinetics, and Mechanism of Giant Fullerene Evaporation. *Phys. Rev. Lett.* **2007**, *99*, 175503.
(48) Hernández, E.; Meunier, V.; Smith, B. W.; Rurali, R.; Terrones, H.; Buongiorno Nardelli, M.; Terrones, M.; Luzzi, D. E.; Charlier, J. C. Fullerene coalescence in nanopeapods: A path to novel tubular carbon. *Nano Lett.* **2003**, *3*, 1037−1042.
(49) López, M. J.; Rubio, A.; Alonso, J. A.; Lefrant, S.; Méténier, K.; Bonnamy, S. Patching and Tearing Single-Wall Carbon-Nanotube Ropes into Multiwall Carbon Nanotubes. *Phys. Rev. Lett.* **2002**, *89*, 255501.
(50) Ding, F.; Yakobson, B. I. Energy-driven kinetic Monte Carlo method and its application in fullerene coalescence. *J. Phys. Chem. Lett.* **2014**, *5*, 2922−2926.
(51) Edwards, W. F.; Thies, M. C. Fractionation of pitches by molecular weight using continuous and semibatch dense-gas extraction. *Carbon* **2006**, *44*, 243−252.
(52) Raj, A.; Man, P. L. W.; Totton, T. S.; Sander, M.; Shirley, R. A.; Kraft, M. New polycyclic aromatic hydrocarbon (PAH) surface processes to improve the model prediction of the composition of combustion-generated PAHs and soot. *Carbon* **2010**, *48*, 319−332.
(53) Marsh, H.; Reinoso, F. R. *Activated carbon*; Elsevier: 2006.
(54) Terrones, H.; Terrones, M. Curved nanostructured materials. *New J. Phys.* **2003**, *5*, 126−126.
(55) Martin, J. W.; Slavchov, R. I.; Yapp, E. K. Y.; Akroyd, J.; Mosbach, S.; Kraft, M. The polarization of polycyclic aromatic hydrocarbons curved by pentagon incorporation: the role of the flexoelectric dipole. *J. Phys. Chem. C* **2017**, *121*, 27154−27163.

DOI: 10.1021/acs.est.8b06861
Environ. Sci. Technol. 2019, 53, 3538−3546